Mon. Not. R. Astron. Soc. **366,** 953–968 (2006) doi:10.1111/j.1365-2966.2005.09772.x

Multiwavelength *XMM–Newton* observations of the Laor et al. sample of PG quasars

C. Brocksopp,[1]⋆ R. L. C. Starling,[2] P. Schady,[1] K. O. Mason,[1] E. Romero-Colmenero[3] and E. M. Puchnarewicz[1]

[1]*Mullard Space Science Laboratory, University College London, Holmbury St Mary, Dorking, Surrey RH5 6NT*
[2]*Astronomical Institute 'Anton Pannekoek', University of Amsterdam, Kruislaan 403, 1098 SJ Amsterdam, the Netherlands*
[3]*South African Astronomical Observatory, PO Box 9, Observatory 7935, Cape Town, South Africa*

Accepted 2005 October 20. Received 2005 October 19; in original form 2005 March 18

ABSTRACT

We present *XMM–Newton*/EPIC spectra for the Laor et al. sample of Palomar Green (PG) quasars. We find that a power law provides a reasonable fit to the 2–5 keV region of the spectra. Excess soft X-ray emission below 2 keV is present for all objects, with the exception of those known to contain a warm absorber. However, a single power law is a poor fit to the 0.3–10.0 keV spectrum and instead we find that a simple model, consisting of a broken power law (plus an iron line), provides a reasonable fit in most cases. The equivalent width of the emission line is constrained in just 12 objects but with low ($<2\sigma$) significance in most cases. For the sources whose spectra are well fitted by the broken-power-law model, we find that various optical and X-ray line and continuum parameters are well correlated; in particular, the power-law photon index is well correlated with the FWHM of the Hβ line and the photon indices of the low- and high-energy components of the broken power law are well correlated with each other. These results suggest that the 0.3–10 keV X-ray emission shares a common (presumably non-thermal) origin, as opposed to suggestions that the soft excess is directly produced by thermal disc emission or via an additional spectral component. We present *XMM–Newton* Optical Monitor (OM) data, which we combine with the X-ray spectra so as to produce broad-band spectral energy distributions (SEDs), free from uncertainties due to long-term variability in non-simultaneous data. Fitting these optical–UV spectra with a Comptonized disc model indicates that the soft X-ray excess is independent of the accretion disc, confirming our interpretation of the tight correlation between the hard and soft X-ray spectra.

Key words: galaxies: active – quasars: general – X-rays: galaxies.

1 INTRODUCTION

The launch of *XMM–Newton* has seen great advances in all areas of X-ray astronomy but its multiwavelength capabilities might be considered one of its greatest assets. This is of particular importance when it comes to studying quasars that are well known for emitting at a broad range of frequencies. Different components of the quasar emit in different regions of the electromagnetic spectrum and so multiwavelength analysis is vital.

The 'big blue bump' (BBB), which is observed in the optical–ultraviolet(UV) range, peaking at ∼1000 Å, is thought to be the signature of thermal emission from an accretion disc (e.g. Peterson 1997 and references therein). Above 2 keV, the spectra can be well modelled using a power law, which is assumed to be due to Comptonization of lower-energy photons. The 'soft excess' above the power law, often seen in X-ray spectra of quasars at energies below ∼2–3 keV, has been attributed to the high-energy end of the BBB (although see also Gierliński & Done 2004); various models have been suggested for the origin of this soft X-ray excess such as direct thermal emission from the accretion disc or reprocessing of disc emission (e.g. Peterson 1997 and references therein). Two additional components thought to be present in quasars, but not accessible to *XMM–Newton*, are the infrared bump (assumed to be emission from dust) and the radio jet (e.g. Peterson 1997 and references therein).

The Laor et al. (1994, 1997) complete sample of 23 quasars was chosen from the Bright Quasar Survey (BQS), a subset of the Palomar Green (PG) survey compiled by Schmidt & Green (1983). The PG survey consists of 114 active galactic nuclei (AGN), 92 of which

⋆E-mail: cb4@mssl.ucl.ac.uk

Table 1. Table listing the 23 PG quasars in the Laor et al. sample, their redshifts and Galactic absorption and details of the *XMM–Newton* observations. Measurements of the Galactic absorption have been obtained from Laor et al. (1997 and references therein).

Quasar	Redshift	$nH_{\rm Gal.}$ ($\times 10^{20}$ cm^{-2})	Observation date	*XMM–Newton* revolution	Observation ID	Exposure (PN/MOS; ks)	Count rate (PN, MOS1, MOS2; count s^{-1})
PG 0947+396	0.2060	1.92	2001-11-03	349	0111290101	17.6/21.1	1.68, 0.31, 0.31
PG 0953+414	0.2341	1.12	2001-11-22	358	0111290201	10.6/13.2	3.64, 0.63, 0.60
PG 1001+054	0.1610	2.88	2003-05-04	623	0150610101	9.1/11.6	0.04, 0.01, 0.01
PG 1048+342	0.1670	1.74	2002-05-13	444	0109080701	28.1/32.2	1.12, 0.19, 0.19
PG 1114+445	0.1440	1.94	2002-05-15	445	0109080801	37.8/42.3	0.66, 0.18, 0.17
PG 1115+407	0.1540	1.74	2002-05-17	446	0111290301	15.0/20.3	1.99, 0.29, 0.30
PG 1116+215	0.1765	1.44	2001-12-02	363	0111290401	5.5/8.4	4.79, 0.74, 0.73
PG 1202+281	0.1653	1.72	2002-05-30	453	0109080101	12.9/17.4	2.55, 0.50, 0.50
PG 1216+069	0.3313	1.57	2002-12-18	554	0111291101	14.0/16.5	1.03, 0.19, 0.18
PG 1226+023	0.1583	1.68	2000-06-13	94	0126700301	44.3/58.5	34.82, 1.84, 1.36
PG 1309+355	0.1840	1.01	2002-06-10	458	0109080201	25.2/29.0	0.43, 0.08, 0.08
PG 1322+659	0.1680	2.88	2002-05-11	443	0109080301	8.7/11.6	2.24, 0.33, 0.33
PG 1352+183	0.1520	2.84	2002-07-20	478	0109080401	12.5/14.9	2.19, 0.34, 0.34
PG 1402+261	0.1640	1.42	2002-01-27	391	0109081001	9.1/12.0	2.98, 0.44, 0.44
PG 1411+442	0.0896	1.05	2002-07-10	473	0103660101	27.5/41.1	0.11, 0.02, 0.02
PG 1415+451	0.1140	0.96	2002-12-08	549	0109080501	21.2/24.1	1.36, 0.21, 0.22
PG 1425+267	0.3660	1.54	2002-07-28	482	0111290601	45.9/–	0.63, 0.45, 0.45
PG 1427+480	0.2210	1.69	2002-05-31	453	0109080901	35.2/39.0	1.10, 0.19, 0.20
PG 1440+356	0.0790	0.97	2001-12-23	373	0107660201	24.8/30.4	6.26, 0.78, 0.77
PG 1444+407	0.2673	1.09	2002-08-11	489	0109080601	18.7/21.5	0.91, 0.13, 0.13
PG 1512+370	0.3707	1.40	2002-08-25	496	0111291001	17.6/20.4	1.45, 0.28, 0.29
PG 1543+489	0.4000	1.68	2003-02-08	580	0153220401	8.2/9.8	0.33, 0.05, 0.05
PG 1626+554	0.1330	1.55	2002-05-05	440	0109081101	5.5/8.9	2.92, 0.44, 0.47

are quasars. With selection criteria $M_B < -23$ and $U - B < -0.44$, the BQS quasars are thought to be representative of most quasars (although see also Jester et al. 2005): because they were selected purely on their optical properties they were also thought to be unbiased in terms of their X-ray properties. In order to create a complete sample, the Laor et al. sample was further constrained by two additional selection criteria:

(i) $z \leqslant 0.400$, in order to prevent the rest frame 0.2 keV being redshifted beyond the range observable by *ROSAT* Position Sensitive Proportional Counter (PSPC); and

(ii) $nH_{\rm Gal} < 1.9 \times 10^{20}$ cm^{-2}, in order to minimize the effects of Galactic absorption.

The full analysis of the *ROSAT* observations was presented in Laor et al. (1997) and suggested that the 0.2–2 keV range of the rest-frame spectrum of a quasar could be fitted by a single power law, with no evidence for any soft excess emission and an upper limit (95 per cent confidence) of $\sim 5 \times 10^{19}$ cm^{-2} on the amount of excess foreground absorption by cold gas. These data also suggested that the mean soft X-ray continuum agreed with an extrapolation of the mean UV continuum. The authors concluded that a thin bare accretion disc model was unable to reproduce the 0.2–2 keV spectral shape (Laor et al. 1997; Zheng et al. 1997).

We have used *XMM–Newton* to update the *ROSAT* observations, providing a much wider X-ray coverage (0.3–10 keV), higher energy resolution and a high signal-to-noise (S/N) ratio, and also providing simultaneous optical and UV data from the Optical Monitor (OM). Our aims were to investigate whether or not claims to the presence of a soft excess, intrinsic absorption and/or iron lines were justified and physical when viewed in the context of the broad-band spectra. We have restricted our observations to the complete Laor et al. sample of 23 quasars but compare our X-ray spectral parameters with those obtained for alternative BQS quasars by Porquet et al. (2004; their sample consisted of 21 PG quasars, 15 of which were Laor objects) and Piconcelli et al. (2005). In this paper, we present the observations in Section 2, the X-ray spectroscopy in Section 3, line and continuum correlations in Section 4, the broad-band spectral energy distributions (SEDs) in Section 5 and discuss our results in Section 6.

2 OBSERVATIONS

XMM–Newton observed the 23 Laor targets between 2001 November and 2003 May and obtained images with each of the three X-ray EPIC cameras (pn, MOS1, MOS2): details of the sources and their observations are listed in Table 1. Each of the three X-ray cameras has a spectral range of 0.2–12 keV, spectral resolution of 20–50 and an angular resolution of ~ 6 arcsec. The EPIC large window mode and thin filter were used (with the exception of PG 1411+442 and 1425+267, which were observed in full frame mode, and PG 1226+023, which was observed with the medium filter and small window mode in order to minimize pile-up). The data were reduced using the SAS v5.4 EPCHAIN and EMCHAIN pipelines for the pn and MOS, respectively. We re-reduced a selection of the sources with the SAS v6.0 version of the software but found it made no significant difference to the subsequent fits. All data sets were inspected for pile-up by comparing the preliminary light curves with the published threshold count rates for each camera, as well as the EPATPLOT routine: PG 1226+023 ($\equiv$ 3C 273) was the only source affected by pile-up. Response matrices and auxiliary files were generated using the RMFGEN and ARFGEN tasks, respectively.

Longer-wavelength images of each quasar were obtained, simultaneously with the X-ray data, using the OM through the optical U, B and V filters and the UV $UVW1$, $UVM2$ and $UVW2$ filters (Mason et al. 2001). They were reduced using the SAS v6.0 OMICHAIN reduction pipeline, which uses an aperture of 12 pixel. We list the

Table 2. Table of optical and UV photometry from the Optical Monitor (OM) observations; statistical errors are given in brackets. Details of the OM and the filters are given in Mason et al. (2001). Flux conversions are stated in the text.

	Filter/magnitudes($\lambda_{\rm eff}$)					
Quasar	*V* (5483 Å)	*B* (4443 Å)	*U* (3735 Å)	*UVW*1 (2910 Å)	*UVM*2 (2310 Å)	*UVW*2 (2120 Å)
PG 0947+396	–	–	15.31 (0.01)	15.13 (0.01)	14.92 (0.01)	14.77 (0.01)
PG 0953+414	–	–	–	13.16 (0.01)	13.71 (0.01)	13.55 (0.01)
PG 1001+054	–	–	–	–	–	–
PG 1048+342	16.51 (0.03)	16.80 (0.02)	15.66 (0.01)	15.44 (0.01)	15.36 (0.02)	15.25 (0.02)
PG 1114+445	15.78 (0.01)	16.17 (0.01)	15.08 (0.01)	15.00 (0.01)	15.15 (0.01)	15.08 (0.02)
PG 1115+407	–	16.00 (0.01)	14.83 (0.01)	14.54 (0.01)	14.25 (0.01)	14.12 (0.01)
PG 1116+215	–	14.32 (0.01)	–	12.85 (0.01)	–	12.43 (0.01)
PG 1202+281	16.27 (0.03)	16.52 (0.02)	15.32 (0.01)	15.10 (0.02)	14.98 (0.02)	14.80 (0.03)
PG 1216+069	15.43 (0.01)	15.64 (0.01)	14.60 (0.01)	14.46 (0.01)	14.20 (0.01)	14.13 (0.01)
PG 1226+023	12.64 (0.01)	12.94 (0.01)	11.77 (0.01)	11.49 (0.01)	11.33 (0.01)	11.28 (0.01)
PG 1309+355	15.64 (0.01)	16.03 (0.01)	15.00 (0.01)	14.84 (0.01)	14.76 (0.01)	14.70 (0.02)
PG 1322+659	–	–	14.82 (0.01)	14.58 (0.01)	14.36 (0.01)	14.27 (0.02)
PG 1352+183	16.37 (0.03)	16.63 (0.02)	15.41 (0.01)	15.14 (0.01)	14.98 (0.02)	14.85 (0.03)
PG 1402+261	–	–	–	14.04 (0.01)	13.74 (0.01)	13.61 (0.01)
PG 1411+442	–	–	13.69 (0.01)	–	–	–
PG 1415+451	15.96 (0.02)	16.54 (0.01)	15.43 (0.01)	15.18 (0.01)	15.15 (0.02)	15.02 (0.02)
PG 1425+267	17.16 0.04	17.17 (0.02)	16.05 (0.01)	16.10 (0.01)	15.90 (0.02)	15.79 (0.03)
PG 1427+480	16.63 0.04	–	15.69 (0.01)	15.53 (0.01)	15.40 (0.01)	15.22 (0.02)
PG 1440+356	14.63 (0.01)	–	13.92 (0.01)	13.66 (0.01)	13.54 (0.01)	13.43 (0.01)
PG 1444+407	15.94 (0.02)	16.07 (0.01)	14.95 (0.01)	14.81 (0.01)	14.48 (0.01)	14.39 (0.02)
PG 1512+370	16.65 (0.03)	16.75 (0.01)	15.67 (0.01)	15.58 (0.01)	15.06 (0.02)	14.85 (0.02)
PG 1543+489	–	–	16.50 (0.01)	–	15.14 (0.01)	–
PG 1626+554	15.79 (0.02)	–	–	14.60 (0.01)	14.49 (0.01)	14.43 (0.02)

central wavelength of the filters and resultant photometry in Table 2. Finally, the magnitudes were corrected for Galactic extinction using the extinction law of Cardelli, Clayton & Mathis (1989) and flux calibrated with respect to Vega. Flux conversions were obtained using the formula $M_{\rm Vega} - M_{\rm quasar} = -2.5\ \log\ (F_{\rm Vega}/F_{\rm quasar})$, where Vega has a brightness of 0.03 mag in the *B* and *V* filters, 0.025 mag in the *U* and UV filters, and fluxes of 3.2652743, 5.9712835, 3.1594819, 3.7391873, 4.4609810, 5.3884371 $\times\ 10^{-9}$ erg cm^{-2} s^{-1} Å^{-1} for the *V*, *B*, *U*, *UVW*1, *UVM*2 and *UVW*2 filters, respectively.[1]

3 X-RAY SPECTROSCOPY

The task XMMSELECT was used to extract an X-ray spectrum from a circular region centred on the source. Further circular regions were positioned on source-free areas of sky to provide a background sample. We corrected for the pile-up in PG 1226+023 by running the SAS V6.0 chains and extracting the spectrum from an annulus centred on the centre of the source. Photons with pattern 0–4 and 0–12, for the pn and MOS respectively, and with quality flag 0 were included. GRPPHA was used to bin the data using a minimum of 20 counts in each bin and 150 counts per bin in the case of PG 1626+554. The extracted spectra were analysed using the XSPEC spectral fitting package (Arnaud 1996).

Initial fits were made using a simple absorbed power law, taking into account both Galactic absorption (obtained from Laor et al. 1997 and references therein) and possible redshifted absorption intrinsic to the quasar. We restricted the energy range to 0.3–10 keV in the observed frame for which the instrument response is generally well known. However, it was clear that there was a significant discrepancy between the pn and MOS spectra with as much as a 10 per cent higher value of the power-law photon index for the pn relative to that of the MOS. Kirsch (2003) outlines two possible explanations for this problem. The first is a gradual change in the MOS response from revolution 200 and, particularly, 450 onwards (as discussed by Porquet et al. 2004). The second factor is a ∼10 per cent higher flux for the pn in the 0.3–1.0 keV range compared with the MOS, which is possibly due to uncertainties in the vignetting and CCD quantum efficiency. Because our sources are all relatively soft, we suggest that both factors are contributing to the discrepancy. While the first factor is an uncertainty with the MOS calibration, we note that the second factor is not necessarily restricted to the MOS. We therefore do not discard all the MOS data (contrary to Porquet et al. 2004) but discard only the MOS data below 0.7 keV. We find that the pn and MOS are in good agreement (typically to within 90 per cent confidence contours) above this energy. We re-reduced four sources chosen at random using the SAS V6.0 software and found that there was no significant improvement in pn/MOS agreement.

We then performed power-law fits to the spectra, fitting pn and MOS simultaneously and restricting the energy range to 2–5 keV in the rest frame (in contrast to Porquet et al. 2004). We included only the effect of Galactic absorption and note that this region of the spectrum is useful for preliminary fits, because it is typically thought to be free of model components due to soft excess, absorption, reflection or emission lines. A power law was indeed a good fit to the spectra in this range and the resultant parameters are listed in Table 3. The values of Γ fall in the range 1.4–2.6, with the exception of PG 1001+054 and 1411+442. Extrapolating the 2–5 keV fit to the full *XMM–Newton* range confirms the result of Porquet et al. (2004) that a soft excess is present in all cases, except for those complicated by the presence of a warm absorber (Ashton et al. 2004; Ashton et al., in preparation).

Indeed, over the full *XMM–Newton* energy range (0.3–10 keV), a simple absorbed power law is not a good fit to the data (see χ^2_ν in final column of Table 3). Many of the sources show excess emission

[1] http://xmm.vilspa.esa.es/sas/documentation/watchout/uvflux.shtml

Table 3. Table of parameters resulting from a single power-law fit to the 2–5 keV energy range (rest frame; column 2 lists the equivalent observed frame energies), including only Galactic absorption. The penultimate column lists the luminosity of each quasar, assuming a standard *WMAP* cosmology. Clearly a power-law spectrum is a reasonable assumption in this region of the spectrum for the majority of the sources. The final column shows the reduced χ^2 for a power-law-model fit to the full 0.3–10 keV range. Clearly this is a poor fit in all cases.

Quasar	Observed frame energy (keV)	Photon index	χ^2 (d.o.f.)	χ^2_ν	Probability	Luminosity ($\times 10^{44}$ erg s^{-1})	χ^2_ν (0.3–10 keV)
PG 0947+396	1.7–4.1	$2.10^{+0.08}_{-0.08}$	279.89 (286)	0.98	0.59	1.18	1.38
PG 0953+414	1.6–4.1	$2.19^{+0.07}_{-0.07}$	302.43 (290)	1.04	0.30	2.89	1.65
PG 1001+054	1.7–4.3	$0.14^{+0.46}_{-0.38}$	1.14 (8)	0.14	1.00	0.025	4.02
PG 1048+342	1.7–4.3	$1.96^{+0.09}_{-0.09}$	194.69 (213)	0.91	0.81	0.55	1.45
PG 1114+445	1.7–4.4	$1.36^{+0.06}_{-0.05}$	412.14 (443)	0.93	0.85	0.57	4.64
PG 1115+407	1.7–4.3	$2.34^{+0.10}_{-0.10}$	170.59 (192)	0.89	0.86	0.50	1.55
PG 1116+215	1.7–4.2	$2.22^{+0.09}_{-0.09}$	226.40 (217)	1.04	0.32	1.79	1.51
PG 1202+281	1.7–4.3	$1.76^{+0.07}_{-0.07}$	290.70 (342)	0.85	0.98	1.36	1.54
PG 1216+069	1.5–3.8	$2.02^{+0.12}_{-0.12}$	184.09 (142)	1.30	0.01	2.14	1.97
PG 1226+023	1.7–4.3	$1.64^{+0.01}_{-0.01}$	1425.47 (864)	1.65	1e-13	27.0	4.99
PG 1309+355	1.7–4.2	$1.80^{+0.11}_{-0.11}$	121.05 (137)	0.88	0.83	0.34	1.74
PG 1322+659	1.7–4.3	$2.34^{+0.13}_{-0.13}$	120.17 (117)	1.03	0.40	0.64	1.48
PG 1352+183	1.7–4.3	$2.10^{+0.11}_{-0.11}$	142.59 (146)	0.98	0.56	0.66	1.39
PG 1402+261	1.7–4.3	$2.42^{+0.10}_{-0.10}$	185.92 (189)	0.98	0.55	0.82	1.63
PG 1411+442	1.8–4.6	$0.34^{+0.19}_{-0.31}$	46.84 (40)	1.17	0.21	0.02	7.33
PG 1415+451	1.8–4.5	$2.14^{+0.09}_{-0.09}$	174.80 (195)	0.90	0.85	0.21	1.68
PG 1425+267	1.5–3.7	$1.49^{+0.07}_{-0.07}$	436.24 (379)	1.15	0.02	3.05	1.47
PG 1427+480	1.6–4.1	$2.04^{+0.07}_{-0.07}$	296.92 (327)	0.91	0.88	0.89	1.45
PG 1440+356	1.9–4.6	$2.41^{+0.06}_{-0.07}$	315.64 (363)	0.87	0.96	0.26	2.24
PG 1444+407	1.6–3.9	$2.37^{+0.14}_{-0.13}$	141.24 (116)	1.22	0.06	0.76	1.45
PG 1512+370	1.5–3.6	$1.95^{+0.08}_{-0.08}$	247.66 (240)	1.03	0.35	4.69	1.33
PG 1543+489	1.4–3.6	$2.54^{+0.35}_{-0.26}$	29.16 (33)	0.88	0.66	0.71	1.10
PG 1626+554	1.8–4.4	$2.01^{+0.10}_{-0.10}$	30.45 (39)	0.78	0.83	0.85	1.68

in the low- and/or high-energy regions of the spectrum. Again, this confirms the results of Porquet et al. (2004) and Piconcelli et al. (2005), so we do not repeat the work here. Instead, we try fitting a broken power law, again including Galactic absorption and possible intrinsic, redshifted absorption (Fig. 1). This gives a more acceptable fit ($0.94 \leqslant \chi^2_\nu \leqslant 1.13$), with the exception of PG 1114+445, 1216+069, 1226+023 and 1411+442 as discussed below (Table 4). Intrinsic broad-band absorption is not required in the majority of our sources, although Porquet et al. (2004) included narrow absorption edges for some objects. Values of the photon index for the low-energy power law fall in the 2.0–4.0 range; for the high-energy power law, the photon indices lie in the range 1.5–2.9 (again with the exceptions of PG 1001+054 and 1411+442). The break energy was in the range 0.7–2.1 keV (or 0.9–2.5 keV in the rest frame).

We also include a single iron line of width 0.01 or 1.0 keV in our model, placing it at each of the three energies 6.4, 6.5 and 6.7 keV (Table 5). However, we find that the equivalent widths of any potential narrow or broad lines can be constrained in just 12 sources: with most of these detections having a significance of $< 2\sigma$, it is debateable as to whether these lines can be considered real. The 99 per cent confidence upper limits to the equivalent width are also listed in Table 5. The central energies of the detected lines are typically consistent with 6.4 or 6.5 keV, corresponding to neutral and weakly ionized iron emission. A more detailed search for iron emission in PG 1226+023 has been published by Page et al. (2004a) and a weak broad line found by co-adding spectra. We note that Jiménez-Bailón et al. (2005) study a sample of 38 PG quasars and detect iron lines in 20 of them, 13 of which are included in the Laor et al. sample. This does not necessarily contradict our results as these authors use a variety of different models, some of which we show in Sections 4–6 may be inappropriate. Further discussion of the iron lines in these sources, with reference to reflection models, can also be found in Porquet et al. (2004).

Alternative models, such as blackbody, bremsstrahlung, Comptonization and more complicated absorption components, are often used to improve fits. Porquet et al. (2004) and Piconcelli et al. (2005) have performed detailed fitting of these models to subsets of the Laor et al. sample and so we do not repeat their work. These authors found that the addition of blackbody or bremsstrahlung model components improved fits but that no single model was able to fit all the objects. The values of the resultant parameters were also regarded as phenomenological rather than physical, in particular requiring temperatures much higher than those thought to be reached in an accretion disc (Piconcelli et al. 2005). Comptonization models tended to be more successful and provided a good fit to the soft

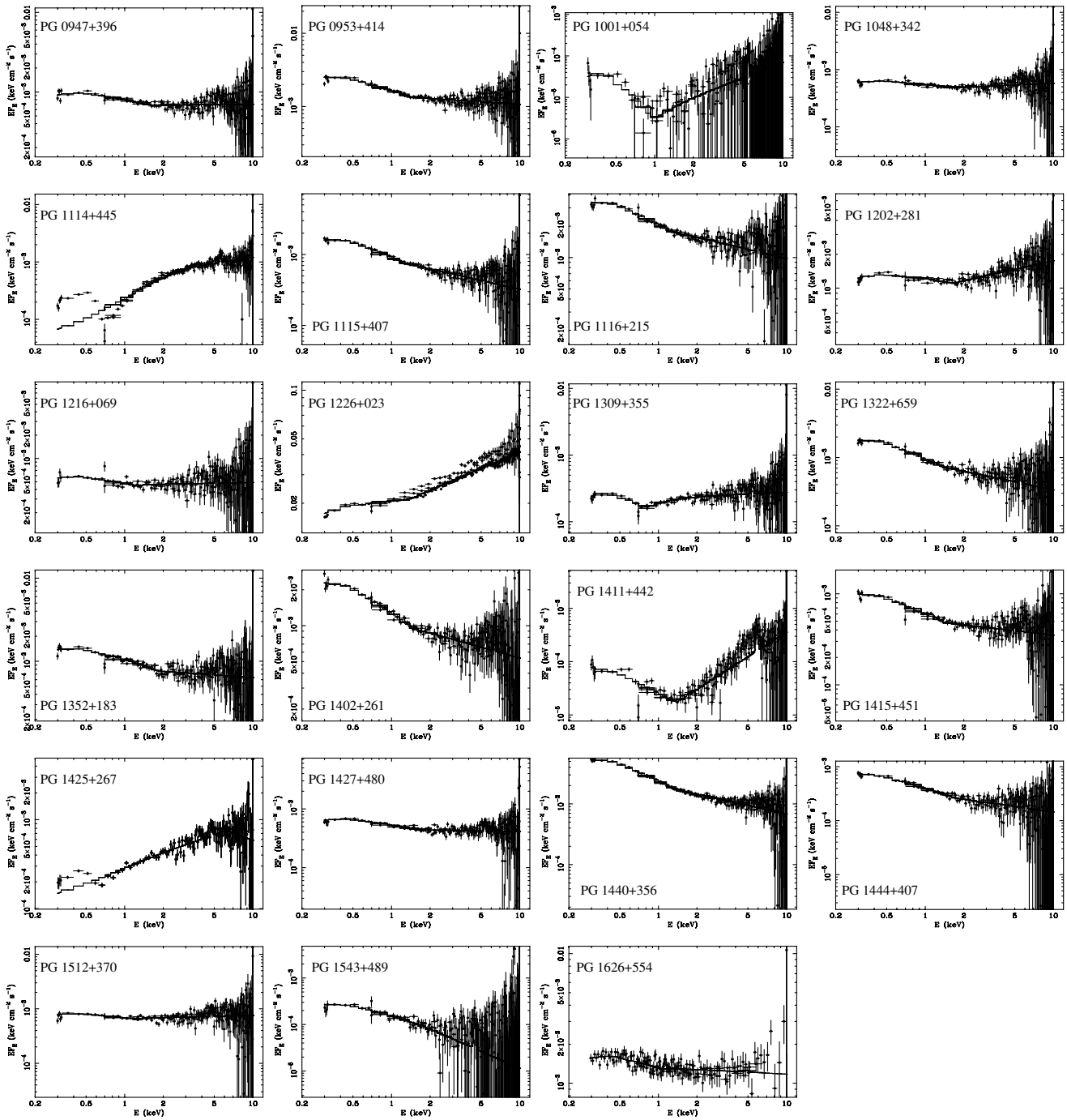

Figure 1. A plot for each quasar showing the X-ray spectra (pn and MOS) in νF_ν space and the best fit to a model comprising an absorbed (allowing for both Galactic and intrinsic absorption) broken power law plus iron line. This simple model provides a good fit to the spectra for the majority of the sources. We note that Ashton et al. (2004) have also included a warm absorber component in order to fit PG 1114+445 and 1309+355 successfully and we suspect that similar detailed modelling would be required in order to fit the spectra of PG 1425+267 and 1411+442 (Ashton et al., in preparation).

excess of the PG quasars (Gierliński & Done 2004; Piconcelli et al. 2005; Porquet et al. 2004). While the Comptonization of disc photons is indeed a potential physical model, there are still problems in that the resultant temperatures lie in an unrealistically narrow range (0.1–0.2 keV), which does not reflect the wider range of probable disc temperatures, and the soft X-ray emitting region would have to be extremely compact ($R \sim 10^{12}$ cm).

The few sources that are not well described by the simple broken-power-law model merit further discussion. Ashton et al. (2004) perform detailed modelling of PG 1114+445 and 1309+355 and require the addition of a warm absorber component. PG 1425+267 is qualitatively similar to PG 1309+355 and may also require an additional absorption component (as suggested previously by Reeves & Turner 2000). PG 1001+054 and 1411+442 are significantly different from the other sources: PG 1411+442 in particular appears to require an additional high-energy component, perhaps reflection which would be consistent with the apparent strong emission line present in this source. Broken-power-law fits to the spectra of PG

Table 4. Model fit to the 0.3–10 keV (observed frame) data using an absorbed broken power law with the addition of a single iron line of width 0.01 keV in the 5.5–8.0 keV (rest frame) range. The observed luminosity in this energy range has also been listed. This model provides a reasonably good fit for the majority of sources with the most notable exceptions being PG 1114+445 (see Ashton et al. 2004) and PG 1411+442 (which is unconstrained; see Ashton et al., in preparation).

Quasar	PhoInd. 1	PhoInd. 2	Break E (keV)	Absorption ($\times10^{20}$ cm^{-2})	Cont. norm. ($\times10^{-3}$)	Luminosity ($\times10^{44}$ erg s^{-1})	χ^2 (d.o.f.)	χ^2_ν	Probability
PG 0947+396	$2.43^{+0.07}_{-0.03}$	$1.87^{+0.13}_{-0.09}$	$2.02^{+0.30}_{-0.44}$	<0.63	0.84	5.4	786.29 (790)	1.00	0.53
PG 0953+414	$2.65^{+0.12}_{-0.03}$	$2.07^{+0.06}_{-0.08}$	$1.56^{+0.22}_{-0.19}$	<1.54	1.69	15.7	826.15 (777)	1.06	0.11
PG 1001+054	$4.36^{+1.72}_{-0.54}$	$0.74^{+0.40}_{-0.39}$	$1.03^{+0.21}_{-0.16}$	<3.35	0.01	0.1	27.79 (26)	1.07	0.37
PG 1048+342	$2.39^{+0.11}_{-0.04}$	$1.84^{+0.06}_{-0.09}$	$1.66^{+0.30}_{-0.14}$	<1.56	0.56	2.0	714.16 (675)	1.06	0.14
PG 1114+445	–	–	–	–	–	–	–	–	–
PG 1115+407	$2.99^{+0.17}_{-0.11}$	$2.36^{+0.06}_{-0.17}$	$1.35^{+0.22}_{-0.13}$	<2.75	0.96	3.3	608.14 (649)	0.94	0.87
PG 1116+215	$2.76^{+0.19}_{-0.04}$	$2.19^{+0.08}_{-0.08}$	$1.46^{+0.22}_{-0.22}$	<1.96	2.13	10.3	702.85 (677)	1.04	0.24
PG 1202+281	$2.27^{+0.04}_{-0.03}$	$1.71^{+0.05}_{-0.05}$	$1.70^{+0.14}_{-0.17}$	<0.50	1.24	5.5	889.89 (902)	0.98	0.61
PG 1216+069	$3.09^{+0.32}_{-0.20}$	$1.97^{+0.08}_{-0.08}$	$0.96^{+0.17}_{-0.06}$	$4.25^{+7.55}_{-2.59}$	0.39	2.3	655.40 (480)	1.37	2e-7
PG 1226+023	$2.04^{+0.01}_{-0.01}$	$1.68^{+0.01}_{-0.01}$	$1.34^{+0.03}_{-0.04}$	<0.12	21.52	94.4	4353.74 (2785)	1.56	<1e-13
PG 1309+355	$3.69^{+0.54}_{-0.51}$	$1.83^{+0.07}_{-0.06}$	$0.78^{+0.02}_{-0.04}$	$6.77^{+4.70}_{-2.52}$	0.13	1.3	456.39 (473)	0.96	0.70
PG 1322+659	$3.03^{+0.19}_{-0.09}$	$2.24^{+0.09}_{-0.12}$	$1.49^{+0.15}_{-0.16}$	<2.76	1.00	4.3	476.39 (495)	0.96	0.72
PG 1352+183	$2.61^{+0.05}_{-0.04}$	$1.99^{+0.11}_{-0.07}$	$1.91^{+0.24}_{-0.25}$	<0.55	1.07	3.5	587.43 (561)	1.05	0.21
PG 1402+261	$2.87^{+0.11}_{-0.04}$	$2.23^{+0.09}_{-0.10}$	$1.55^{+0.23}_{-0.14}$	<1.31	1.31	5.4	727.0 (642)	1.13	0.01
PG 1411+442	$3.37^{+0.47}_{-0.15}$	$0.35^{+0.11}_{-0.10}$	$1.34^{+0.09}_{-0.12}$	<0.04	0.02	0.1	308.3 (157)	1.96	6e-12
PG 1415+451	$2.69^{+0.08}_{-0.03}$	$2.03^{+0.09}_{-0.07}$	$1.66^{+0.16}_{-0.21}$	<0.79	0.62	1.2	698.40 (671)	1.04	0.23
PG 1425+267	$3.09^{+0.93}_{-0.39}$	$1.49^{+0.04}_{-0.10}$	$0.67^{+0.05}_{-0.04}$	$4.69^{+8.33}_{-3.31}$	0.16	9.9	438.37 (409)	1.07	0.56
PG 1427+480	$2.48^{+0.04}_{-0.03}$	$1.96^{+0.07}_{-0.07}$	$1.81^{+0.20}_{-0.26}$	<1.27	0.55	4.2	821.74 (843)	0.97	0.69
PG 1440+356	$3.18^{+0.12}_{-0.09}$	$2.43^{+0.07}_{-0.06}$	$1.43^{+0.13}_{-0.13}$	$1.15^{+1.01}_{-0.79}$	2.50	2.2	1007.30 (921)	1.09	0.02
PG 1444+407	$2.84^{+0.11}_{-0.04}$	$2.07^{+0.21}_{-0.20}$	$2.00^{+0.37}_{-0.46}$	<1.34	0.40	5.2	480.77 (460)	1.05	0.24
PG 1512+370	$2.33^{+0.18}_{-0.04}$	$1.85^{+0.09}_{-0.06}$	$1.41^{+0.21}_{-0.34}$	<1.30	0.71	19.1	679.47 (663)	1.02	0.32
PG 1543+489	$3.87^{+1.79}_{-0.67}$	$2.85^{+0.34}_{-0.80}$	$0.90^{+2.25}_{-0.20}$	<32	0.15	4.6	164.93 (158)	1.04	0.34
PG 1626+554	$2.44^{+0.24}_{-0.10}$	$2.05^{+0.06}_{-0.13}$	$1.05^{+0.57}_{-0.16}$	<2.24	1.36	3.6	180.47 (166)	1.09	0.21

1216+069 and 1226+023 are also unacceptable, although in these cases it is not so clear why: the PG 1226+023 spectra are of a much higher S/N ratio than the other sources and this seems to be the reason why the fit is not as successful (suggesting, perhaps, that higher S/N ratio observations of the other sources would also require more sophisticated models). Detailed modelling of individual sources is beyond the scope of this paper but will be addressed in follow-up work.

4 X-RAY/OPTICAL CONTINUUM AND LINE LUMINOSITY CORRELATIONS

We have plotted various combinations of spectral parameters and line and continuum[2] luminosities in Figs 2 and 3. The optical data were obtained from Laor et al. (1997) but we note that the lack of simultaneous observations of any varying sources is more likely to weaken the correlations than to strengthen them. We then calculated the associated Spearman rank order correlation coefficients (ρ): many of the plots show only scatter, but there are also a number of significant correlations ($0.6 \leqslant \rho < 0.9$ to within 99 per cent confidence). We list these higher values of ρ in Table 6. We note that PG 1114+445 has been omitted from the plots on account of its extremely poor fits to the broken-power-law model. For each pair of parameters in the table, the first value of ρ is for the plots from Figs 2 and 3; the second value is obtained through further omission of PG 1001+054, 1216+069, 1411+442, 1309+355 and 1425+267, sources which have been labelled 'X-ray weak' by Laor et al. (1997), shown to contain a warm absorber (e.g. Reeves & Turner 2000; Ashton et al. 2004) or for which the broken power law provides an inadequate fit to the spectrum.

Allowing for the few discrepant sources that require a more complicated model, it is clear that there are a number of strong correlations present. In Fig. 2, we show that both the hard and soft photon indices are correlated with the [O III] luminosity and the Hβ FWHM. The break energies do not show any form of correlated behaviour with other quantities. Similarly the 3000-Å and Hβ luminosities do not seem to show any dependency on the X-ray spectral parameters. Fig. 3 shows that the 2.0- and 10.0-keV luminosities are clearly correlated with all four optical parameters; the 0.3 keV luminosities are not correlated with any of the optical parameters.

These results confirm the results of Brandt, Mathur & Elvis (1997), Laor et al. (1997) and Reeves & Turner (2000), who find similar correlations, most notably the result that the X-ray spectrum steepens as the FWHM of the Hβ line decreases. Reeves & Turner (2000) suggest that, because objects with narrower Hβ lines

[2] Here, we use only the luminosity derived using the pn data because the MOS spectra were unreliable at 0.3 keV.

Table 5. Equivalent widths of a single possible iron line, of width 0.01 or 1.0 keV and rest-frame energies 6.4, 6.5 or 6.7 keV, of an absorbed broken-power-law model. Upper limits on the equivalent width are to within 99 per cent. We note that Page et al. (2004a) detected a weak, broad line in PG 1226+023 on co-adding a number of different observations.

Quasar	EW (0.01 keV) 6.4 keV	EW (0.01 keV) 6.5 keV	EW (0.01 keV) 6.7 keV	EW (1.0 keV) 6.4 keV	EW (1.0 keV) 6.5 keV	EW (1.0 keV) 6.7 keV
PG 0947+396	93^{+68}_{-65}	89^{+69}_{-65}	<108	203^{+202}_{-192}	205^{+206}_{-195}	205^{+215}_{-204}
PG 0953+414	<62	<70	<121	<196	<202	206^{+211}_{-203}
PG 1001+054	<2	<2	<2	$<10^6$	$<10^6$	$<10^6$
PG 1048+342	<124	<103	<165	236^{+246}_{-233}	<252	<261
PG 1114+445†	–	230^{+90}_{-70}	–	–	–	–
PG 1115+407	<155	<166	125^{+126}_{-121}	462^{+324}_{-318}	488^{+336}_{-329}	534^{+358}_{-352}
PG 1116+215	<99	<88	101^{+102}_{-97}	300^{+270}_{-259}	316^{+278}_{-267}	340^{+293}_{-281}
PG 1202+281	<84	<61	<43	<16	<172	<180
PG 1216+069	<168	<152	<172	298^{+311}_{-265}	310^{+318}_{-271}	332^{+333}_{-284}
PG 1226+023	9^{+6}_{-7}	<12	9^{+7}_{-7}	53^{+24}_{-24}	51^{+25}_{-25}	44^{+26}_{-26}
PG 1309+355	137^{+155}_{-116}	<223	<224	<382	<385	<394
PG 1322+659	<280	178^{+178}_{-159}	<273	<431	<447	<473
PG 1352+183	<187	<186	<194	<329	<337	<352
PG 1402+261	<186	<169	<162	446^{+312}_{-302}	481^{+321}_{-313}	544^{+342}_{-334}
PG 1411+442	<706	<683	<428	<706	<683	<428
PG 1415+451	<183	<170	117^{+115}_{-104}	<300	<307	<319
PG 1425+267	<113	<146	<114	<213	<214	<209
PG 1427+480	<110	<128	<108	<183	<188	<195
PG 1440+356	<136	<152	<131	424^{+246}_{-240}	449^{+254}_{-250}	494^{+273}_{-268}
PG 1444+407	<150	<197	<217	<364	<370	<386
PG 1512+370	74^{+69}_{-59}	81^{+71}_{-62}	<131	210^{+205}_{-176}	219^{+208}_{-180}	231^{+217}_{-186}
PG 1543+489	<169	<174	<204	$<10^6$	$<10^6$	$<10^6$
PG 1626+554	<344	<401	<376	<486	<512	<572

†The equivalent width for PG 1114+445 is obtained from Ashton et al. (2004) who include a warm absorber in the model.

are thought to accrete at a higher fraction of the Eddington limit, there is greater Compton cooling of the hard X-ray-emitting corona and thus a steepening of the spectrum. They also suggest that a soft excess component associated with the accretion disc should therefore be present in the objects with narrower lines. However, we find that the soft excess is actually present below 2 keV in *all* sources in the Laor et al. sample that do not contain some sort of warm absorber. Instead, in Fig. 4, we compare the photon indices of the low- and high-energy power laws used in our broken-power-law fits and find a strong correlation, confirming the result of Porquet et al. (2004): $\rho = 0.97$ (to within >99 per cent confidence) is obtained when we omit the (consistently discrepant) sources PG 1001+054, 1411+442, 1216+069, 1309+355 and 1425+267. We note that the correlation is stronger for our sample than for that of Porquet et al. (2004), who obtain $\rho = 0.85$: this may be a reflection either on the slightly different sample or on our use of the broken power law, instead of fixed energy ranges in the observed frame. We discuss the implications of this correlation further in Section 6.

5 SPECTRAL ENERGY DISTRIBUTIONS

The most comprehensive compilations of AGN/quasar SEDs presented to date are those of Elvis et al. (1994) and Kuraszkiewicz et al. (2003). These authors included 2–10 keV X-ray data obtained by the *HEAO* missions, archive data obtained from the literature and Kuraszkiewicz et al. (2003) also presented far-infrared *Infrared Space Observatory* (*ISO*) data. In particular, the Kuraszkiewicz et al. (2003) sample is hard X-ray selected, which is unbiased by effects due to obscuration and reprocessing.

The Laor et al. (1997) sample was optically selected with the intent of defining a representative sample of X-ray properties; however, we note that this has the effect of biasing the sample against obscured sources, as discussed by Kuraszkiewicz et al. (2003). None the less, the quality of the *XMM–Newton* data that we present here is sufficiently superior to the *HEAO* data that compiling SEDs is a valuable exercise, even if the multiwavelength results cannot be considered representative of all quasars.

In Fig. 5, we plot the optical–X-ray spectra (OM photometry plus EPIC spectra) for each quasar in the Laor et al. sample. They have been plotted in νF_ν space in Fig. 5 and have been corrected for Galactic absorption. Clearly, the plots show a wide range of spectral shapes and we discuss this in detail below.

The SEDs are dominated, as expected (e.g. Elvis et al. 1994), by the BBB in the optical–UV region. The turnover of the BBB is not observed for any of the Laor et al. sample. However, as already noted, the majority of the X-ray spectra show a soft excess. Analysis of *ROSAT* data by Puchnarewicz et al. (1996 and references therein) revealed evidence for correlations between the optical and X-ray

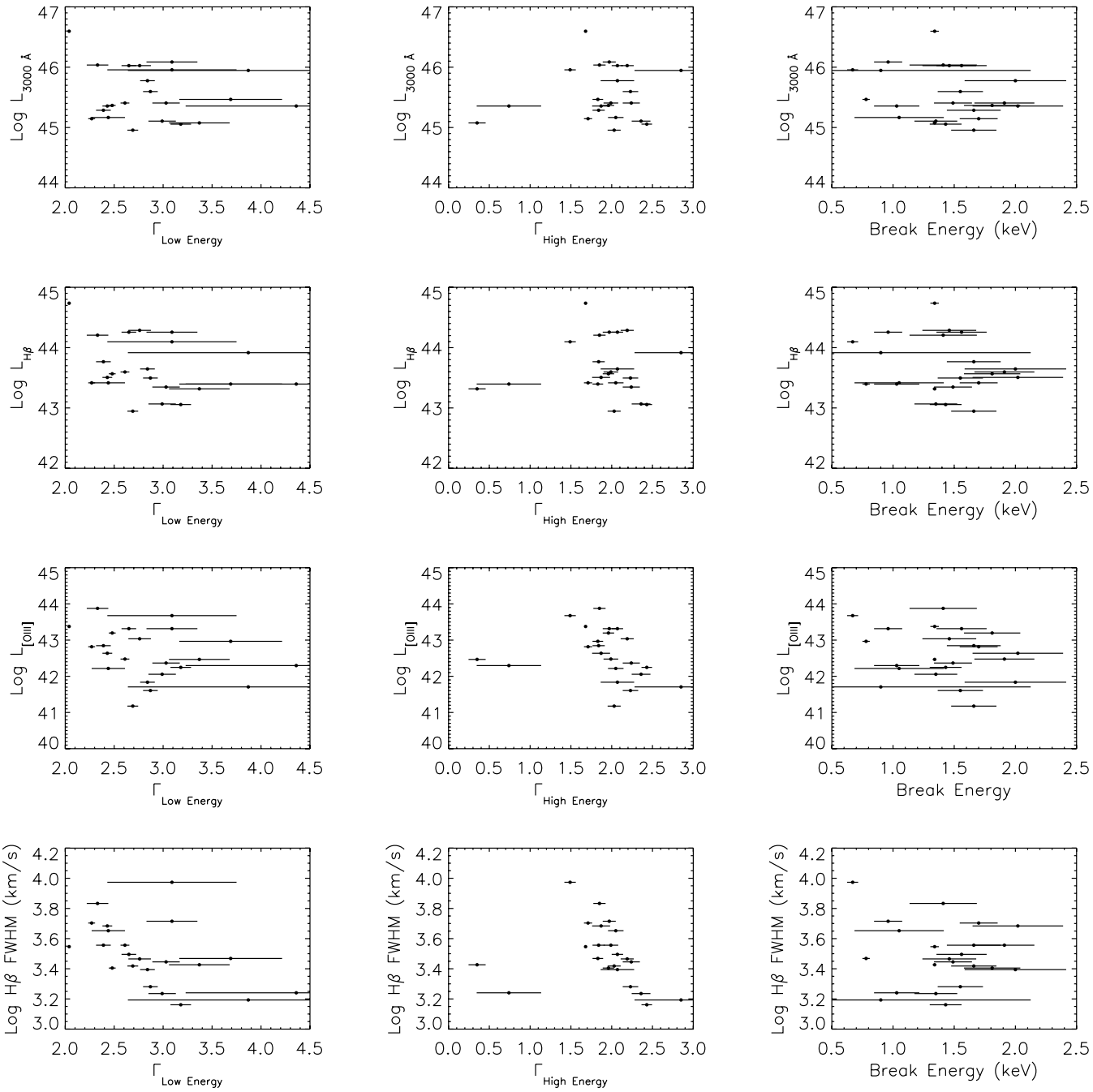

Figure 2. Scatter plots showing various optical parameters (obtained from Laor et al. 1997) plotted against the broken-power-law parameters obtained in Section 3 (omitting PG 1114+445). The break energies show no indication of correlated behaviours; however, with the exception of PG 1001+054 and 1411+442, the [O III] luminosity and, particularly, the Hβ FWHM are correlated with the photon index, in the sense that, as the spectrum hardens, the [O III] luminosity and Hβ FWHM increase. Spearman rank order correlation coefficients for each plot are listed in Table 6.

spectral slopes and the optical:X-ray flux ratio. Such correlations led to the conclusion that there is a strong behavioural link between the BBB and the soft X-ray excess. The additional correlations reported in Section 4 and references therein support this conclusion. The correlation between the soft and hard X-ray power-law slopes suggests further still that there must be a behavioural link between the BBB and the X-ray spectrum as a whole, as opposed to the soft excess in isolation.

We have fitted our *XMM–Newton*-OM photometry with Comptonized accretion disc curves generated by a modified Czerny & Elvis (1987) model (Siemiginowska et al. 1995; Starling et al. 2004). The accretion disc spectra are calculated assuming that the disc is geometrically thin, emitting locally as a modified blackbody (including electron scattering and Comptonization in the atmosphere of the disc) in a Kerr geometry. They do not include the effects of irradiation but are appropriate for simple modelling of the soft excess of X-ray spectra. The best-fitting models are plotted on top of the data in Fig. 5 (solid lines) and appear to be a good or reasonable representation of the OM data for a number of objects. The values of χ^2_ν are listed with the best-fitting masses in Table 7; while some

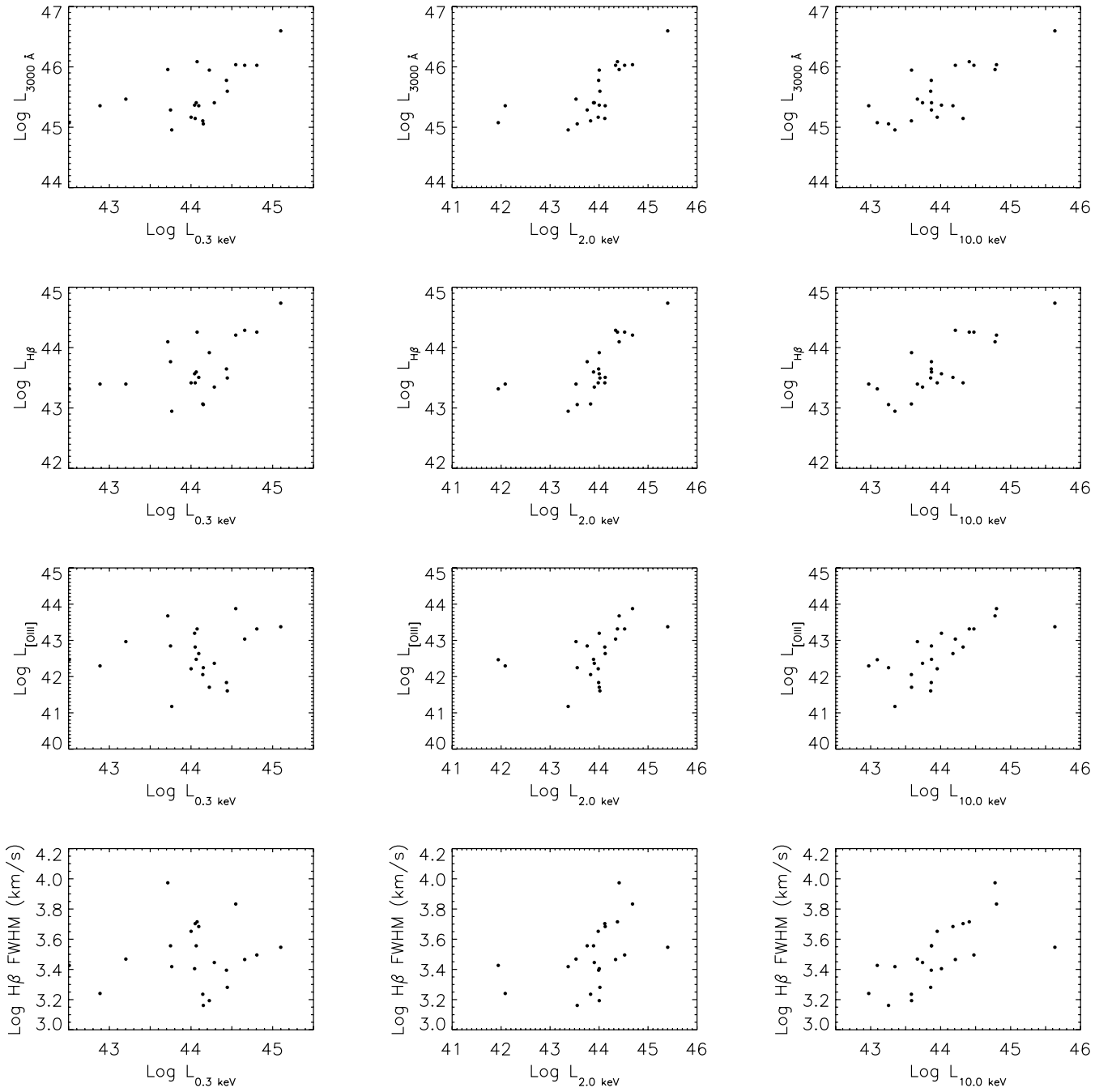

Figure 3. Scatter plots showing various optical parameters (obtained from Laor et al. 1997) plotted against X-ray luminosities at 0.3, 2.0 and 10.0 keV (omitting PG 1114+445). It is clear that, as the 2.0- and 10.0-keV luminosities increase, so too do the values of all four optical parameters; any correlation at 0.3 keV is less convincing, perhaps on account of the EPIC response. Pearson correlation coefficients for each plot are listed in Table 6.

values of χ^2_ν are relatively high, we note that for this preliminary study of the SEDs we have used only a conservative estimate (optical, 1 per cent; UV, 5 per cent) for the flux calibration systematic errors and have relatively few points available for constraining the fits. The results also include estimates of the mass accretion rate and inclination angle; the full range of parameter space is sampled in each case and the results also listed in Table 7. We include approximate error ranges (to within 99 per cent confidence) for the masses but were unable to constrain the mass accretion rate, luminosity or inclination angle. In order to determine the errors, we have obtained the volume in parameter space that is contained within $\Delta\chi^2$ of the minimum χ^2 for each fit. However, these error ranges should be used with caution because they do not reflect exactly those points of parameter space that were included within the $\Delta\chi^2 + \chi^2_{\rm min}$ volume.

It is clear from Fig. 5 that, despite reasonable fits to the OM data, the Kerr models often predict an excess of flux compared with the observed X-ray data (6 out of 22 cases). While we might expect this for those sources known to contain warm absorbers, this is not a satisfactory explanation for the remainder (e.g. PG 1115+407). If

Table 6. Spearman rank order correlation coefficients ($\rho \geqslant 0.5$ to 99 per cent confidence) calculated for each of the scatter plots in Figs 2 and 3. Optical/UV luminosities are from Laor et al. (1997) and converted into the *WMAP* equivalent. For each pair of parameters, the first value of ρ is for the plots from Figs 2 and 3. The second value is obtained through further omission of the five discrepant objects: these quasars may be discrepant on account of being an 'X-ray weak quasar' and containing a warm absorber (PG 1001+054, 1309+355, 1411+442 and 1425+267), or on account of being less well fitted by a broken power law than the majority of other sources (PG 1216+069). We note that a number of these correlation coefficients can be increased still further through omission of *only* PG 1001+054 and 1411+442, but do not include these values for consistency with Fig. 4.

	Luminosity (3000 Å)	Luminosity (Hβ)	Luminosity ([O III])	FWHM (Hβ)
Low energy Γ	–	–	$-/-0.66$	$-0.53/-0.86$
High energy Γ	–	–	$-0.52/-0.60$	$-0.52/-0.79$
Break energy	–	–	–	–
Luminosity (0.3 keV)	0.59/0.69	0.52/0.48	–	–
Luminosity (2.0 keV)	0.77/0.77	0.82/0.73	0.63/0.65	0.55/0.45
Luminosity (10.0 keV)	0.67/0.58	0.78/0.66	0.74/0.78	0.78/0.73
Low energy Γ versus high energy Γ: $\rho \sim 0.97$ to 99 per cent confidence (see text and Fig. 4)				

instead we use the published masses from the literature (obtained by line width techniques; Vestergaard 2002; Shields et al. 2003; Baskin & Laor 2005), the fits are much worse ($\gg 3\sigma$ in most cases) and the predicted soft X-ray flux exceeds that observed in seven systems. Most of the masses we derive, by fitting the OM data, are higher than published estimates in the literature: accretion rates in excess of the Eddington limit (and outside the model limits) and/or the effects of, for example, irradiation may be required in order to provide acceptable fits to these published mass values. In 11 objects (e.g. PG 0953+414), the models that use the published masses (dotted lines in Fig. 5) underestimate the optical/UV flux compared with the OM points. This is somewhat worrying because it shows that either the models are inadequate and, for example, irradiation needs to be included, or it is incorrect to assume that there is no significant contribution to the optical flux from, for example, host galaxy contamination and/or emission lines. Alternatively it may suggest that the source luminosity has varied since the mass estimates were published, as would be consistent with the discrepancies between the OM and *International Ultraviolet Explorer* (*IUE*) data in some objects. Finally, we do not confirm the correlation between mass and 2–10 keV luminosity ($\rho \sim 0.5$ to within 99.7 per cent confidence) as found by Piconcelli et al. (2005), using either our derived masses or the published masses of the Laor PG quasars.

The most striking feature of these plots is that there appears to be no relationship between the fits and the X-ray spectra. There is no source for which the soft excess has a sufficiently steep spectrum that it can be reproduced by the disc model, in contrast with a source like Mkn 841 for which a disc spectrum can be fitted to the combined soft excess and UV spectrum (Arnaud et al. 1985). Indeed, we find that the slope and flux of the soft excess is not predicted by the disc model to any significant degree, which provides an interesting challenge for interpreting the optical/UV/X-ray correlations discussed above.

As an alternative, we have also performed fits to the spectra using Schwarzschild models, both with and without modifications to correct for the effects of opacity. The values of χ^2_ν marked with 'm' in Table 7 indicate which of the best-fitting Schwarzschild models had been modified to include the effects of opacity. These fits are shown in Fig. 5 (dashed lines). Schwarzschild models do not predict significant flux in the X-ray region and thus the problem of overestimating the X-ray flux is eliminated. Table 7 shows that the fits to the optical/UV data are improved for the majority of the Laor objects, compared with the Kerr fits ($\Delta\chi^2 > 1.0\sigma$ for 17 objects and

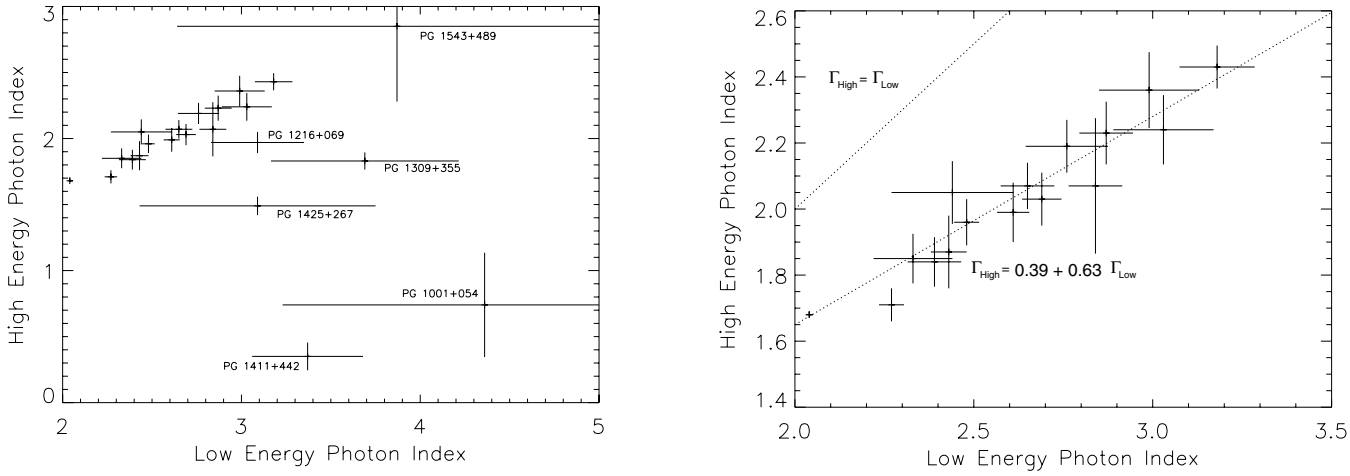

Figure 4. Left-hand side: scatter plot showing the high-energy photon indices plotted against the low-energy photon indices. Clearly, with the exception of the six discrepant objects, there is a strong correlation ($\rho \sim 0.97$ to 99 per cent confidence). This suggests that the regions responsible for the emission are either one and the same, or in direct 'contact' with each other. The discrepant objects are mainly those that contain warm absorbers (Ashton et al. 2004) and/or are defined as 'X-ray weak' (Laor et al. 1997). PG 1216+069 is poorly fitted by the broken power law but it is less clear why it should be discrepant. Right-hand side: expanded view of the highly correlated region of the plot. The dotted lines correspond to $\Gamma_{High} = \Gamma_{Low}$ and $\Gamma_{High} = 0.39 + 0.63\Gamma_{Low}$, where the errors on the intercept and gradient are 0.08 and 0.04, respectively.

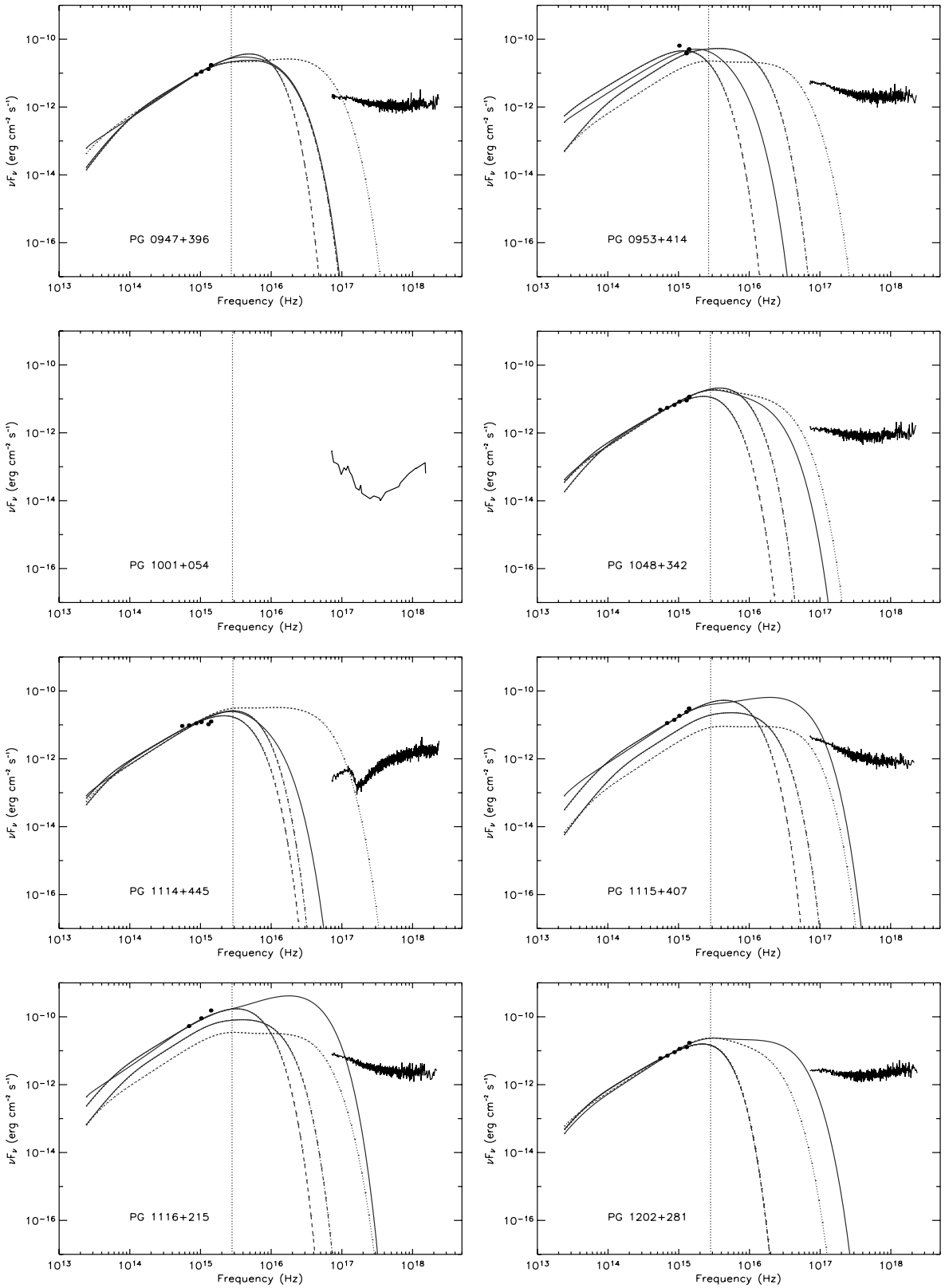

Figure 5. Broad-band optical–X-ray spectra (in the observed frame) for each quasar in the Laor et al. sample. We include the *XMM–Newton* X-ray spectra (lines) and OM photometry (filled circles) studied in this paper. All data have been corrected for Galactic absorption, using the extinction curves of Cardelli et al. (1989) where appropriate. The vertical dotted line represents the Lyman limit for each quasar. The best-fitting Kerr (solid line) and Schwarzschild (dashed line) Comptonized accretion disc models have been overplotted, as have the published-mass Kerr (dotted line) and Schwarzschild (dot-dashed line) models.

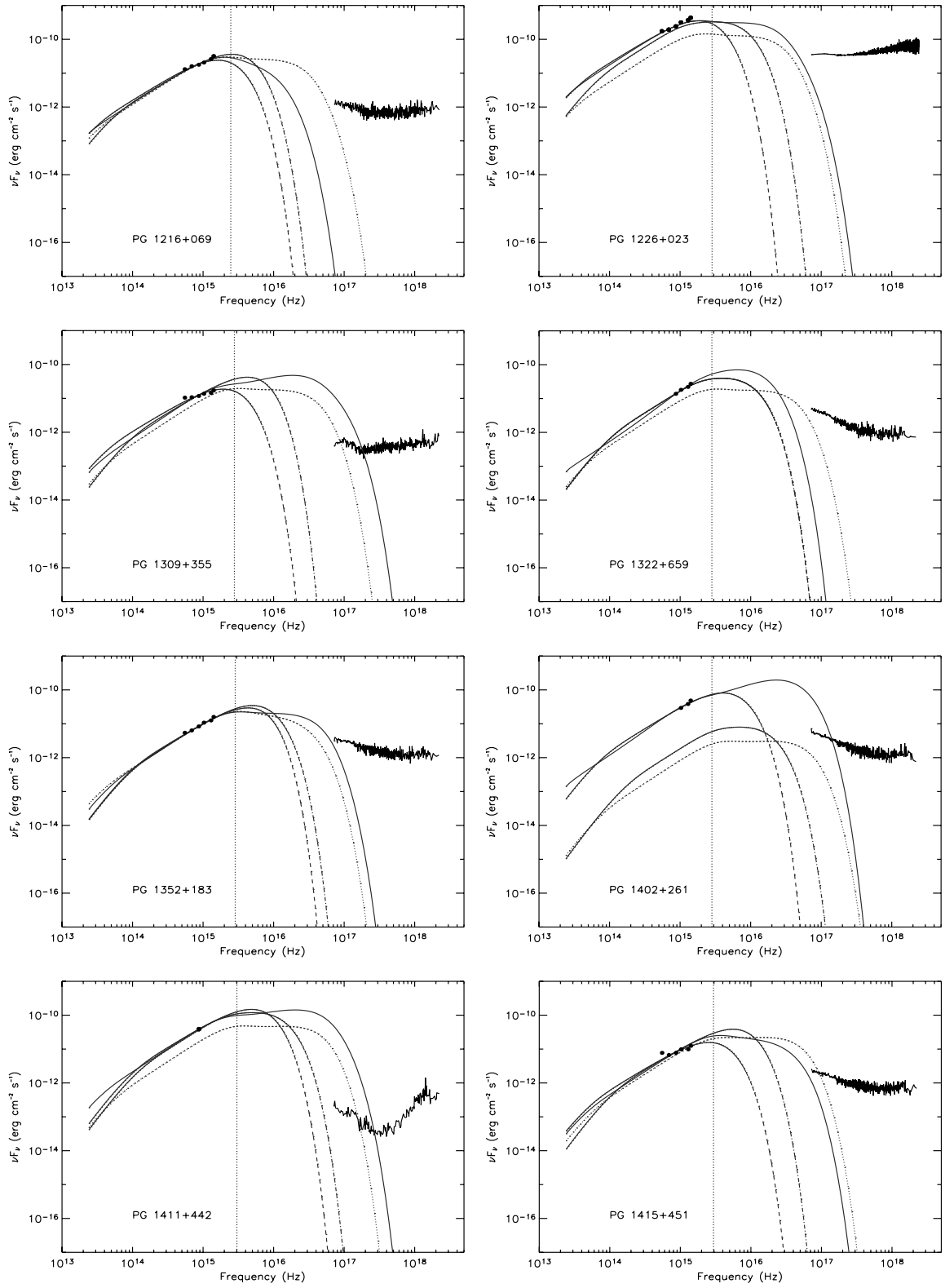

Figure 5 – *continued*

$\Delta\chi^2 > 2.6\sigma$ for 11 objects). There is also a marginal increase in agreement between the masses derived and the published values (dot-dashed lines in Fig. 5).

Similar modelling of subsets of the Laor et al. sample was performed by other authors: we find that our resultant masses are comparable with, although better-constrained than, those of Laor (1990) but are consistently lower than those of Sun & Malkan (1989). We also note that Laor (1990) found that Kerr models were more successful at describing the data. Whilst there is evidence for a rotating black hole in MCG–6-30-15 (Wilms et al. 2001; Vaughan &

Table 7. Results from fitting the Kerr and Schwarzschild SED models to the OM photometry. The first two columns list the sources and the number of degrees of freedom for the fits. The next four columns (first line of data) show the best-fitting mass and χ^2_ν of the Kerr and Schwarzschild models, respectively. The seventh column lists the published mass estimates for each source and the final two columns show the minimum χ^2_ν obtainable for these published masses. Derived masses for which 99 per cent confidence intervals include the published mass values are marked by an asterisk. The values of χ^2_ν marked with 'm' indicate which of the best-fitting Schwarzschild models had been modified to include the effects of opacity. We find that the values of χ^2_ν are relatively high in some cases, but the majority appear to provide reasonably successful representations of the OM data when plotted in Fig. 5. In approximately 50 per cent of the sources (typically those for which $\chi^2_\nu \leqslant 13$), the fits have a probability $\geqslant 0.05$ that the model is an acceptable representation of the data. The second line of data for each source gives the fractional mass accretion rate (Kerr models), fractional luminosity (Schwarzschild models) and the cosine of the inclination angle: the models sampled the full parameter space of these parameters and we include their values for completeness. Note that, in order to determine errors (to within 99 per cent confidence) on the resultant masses, we have obtained the volume in parameter space that is contained within $\Delta\chi^2$ of the minimum χ^2 for each fit. This does not enable us to constrain the values of mass accretion rate, luminosity or inclination angle, but gives us approximate error ranges for the masses. However, these error ranges should be used with caution because they do not reflect exactly those points that were included within the $\Delta\chi^2 + \chi^2_{\rm min}$ volume of parameter space. Published mass estimates for each source from [a]Shields et al. 2003, [b]Vestergaard 2002 and [c]Baskin & Laor 2005.

Quasar	d.o.f.	Best-fitting Kerr BH Mass ($\log M_\odot$) $\dot{M}/\dot{M}_{\rm Edd}\ \cos i$	$\chi^2_{\nu,\,\rm Kerr}$	Best-fitting Schwarzschild BH mass ($\log M_\odot$) $L/L_{\rm Edd}\cos i$	$\chi^2_{\nu,\,\rm Schwarz.}$	Published-mass BH Mass ($\log M_\odot$)	$\chi^2_{\nu,\,\rm Kerr}$ $\dot{M}/\dot{M}_{\rm Edd}\ \cos i$	$\chi^2_{\nu,\,\rm Schwarz.}$ $L/L_{\rm Edd}\cos i$
PG 0947+396	4	$9.1^{+0.1}_{-0.7}$*	1.6	$8.1^{+0.7}_{-0.0}$*	1.6	8.54[a]	2.9	2.1 (m)
		0.10 0.50		1.00 1.0			0.80 0.75	1.0 0.25
PG 0953+414	4	$9.4^{+0.2}_{-0.5}$	20.6	$9.8^{+0.0}_{-0.5}$	15.6 (m)	8.51[a]	174.3	33.8 (m)
		0.10 1.00		0.25 0.1			0.80 1.00	1.0 1.00
PG 1001+054	–	–	–	–		7.65[a]	–	–
		–	–					
PG 1048+342	6	$8.4^{+0.3}_{-0.3}$*	8.0	$8.5^{+0.0}_{-0.1}$	3.3 (m)	8.25[a]	8.3	7.0
		0.20 1.00		0.75 0.1			0.30 1.00	0.4 0.50
PG 1114+445	6	$8.6^{+0.0}_{-0.0}$	74.5	$8.7^{+0.0}_{-0.0}$	37.0	8.41 ± 0.09[b]	85.5	57.3
		0.10 1.00		0.50 0.1			0.50 0.75	0.2 0.75
PG 1115+407	5	$8.8^{+0.2}_{-0.5}$	6.8	$8.5^{+0.1}_{-0.5}$	5.9	7.505[c]	1207.8	627.4 (m)
		0.30 0.50		0.25 0.9			0.80 1.00	1.0 1.00
PG 1116+215	2	$9.7^{+0.2}_{-0.0}$	12.2	$9.1^{+0.1}_{-0.4}$	14.6	8.50 ± 0.10[b]	2196.7	881.0 (m)
		0.30 0.25		0.25 1.0			0.80 1.00	1.0 1.00
PG 1202+281	5	$8.2^{+0.7}_{-0.0}$*	4.0	$8.5^{+0.1}_{-0.4}$*	2.5 (m)	8.12 ± 0.09[b]	6.1	2.5 (m)
		0.70 1.00		1.00 0.1			0.20 1.00	0.1 1.00
PG 1216+069	6	$9.3^{+0.0}_{-0.1}$*	13.0	$9.6^{+0.0}_{-0.4}$*	10.4	9.17 ± 0.15[b]	17.0	13.4
		0.20 1.00		0.25 0.2			0.70 1.00	0.5 0.75
PG 1226+023	28	$9.3^{+0.0}_{-0.0}$	20.8	$9.7^{+0.0}_{-0.0}$	18.3	8.88[a]	2164.2	253.8 (m)
		0.70 1.00		0.25 0.4			0.80 1.00	1.0 1.00
PG 1309+355	5	$9.0^{+0.0}_{-0.6}$	68.4	$8.8^{+0.0}_{-0.1}$	32.6	8.21 ± 0.13[b]	363.2	67.4
		0.80 0.25		0.75 0.1			0.80 1.00	0.7 1.00
PG 1322+659	3	$9.3^{+0.0}_{-0.8}$	1.0	$8.1^{+0.7}_{-0.0}$	1.8 (m)	8.09[a]	358.3	1.8 (m)
		0.10 0.25		1.00 0.8			0.80 1.00	0.8 1.00
PG 1352+183	5	$8.1^{+0.7}_{-0.0}$*	3.1	$8.0^{+0.5}_{-0.2}$*	2.1	8.27 ± 0.09[b]	3.3	3.0
		0.70 1.00		1.00 0.5			0.30 1.00	0.9 0.25
PG 1402+261	2	$9.3^{+0.0}_{-0.8}$	2.7	$8.7^{+0.3}_{-0.5}$	2.7	7.845[c]	490.0	455.1 (m)
		0.30 0.25		0.25 1.0			0.80 1.00	1.0 1.00
PG 1411+442	6	$8.6^{+0.4}_{-0.2}$	1.4	$8.1^{+0.3}_{-0.1}$	0.6	7.87[a]	3139.2	22.7 (m)
		0.60 0.50		0.75 0.8			0.80 1.00	1.0 1.00
PG 1415+451	5	$8.0^{+0.5}_{-0.0}$	55.8	$8.4^{+0.0}_{-0.0}$	35.8	7.81 ± 0.09[b]	99.8	49.1
		0.40 1.00		0.50 0.1			0.80 1.00	0.7 0.75
PG 1425+267	7	$8.9^{+0.4}_{-0.3}$*	6.5	$9.2^{+0.2}_{-0.0}$*	3.8	9.317[c]	7.8	43.5 (m)
		0.20 1.00		0.25 0.2			0.50 0.25	0.1 0.25
PG 1427+480	6	$8.3^{+0.7}_{-0.0}$	4.8	$8.7^{+0.0}_{-0.5}$	2.6 (m)	7.99[a]	223.6	7.4 (m)
		0.70 1.00		0.75 0.1			0.80 1.00	1.0 1.00
PG 1440+356	4	$8.1^{+0.1}_{-0.0}$	95.6	$8.5^{+0.0}_{-0.1}$	51.1	7.30 ± 0.10[b]	2442.3	1854.2 (m)
		0.70 1.00		0.75 0.1			0.80 1.00	1.0 1.00
PG 1444+407	5	$8.7^{+0.4}_{-0.0}$	5.1	$9.1^{+0.0}_{-0.6}$	4.1	8.23 ± 0.10[b]	995.2	328.2 (m)
		0.70 1.00		0.25 0.4			0.80 1.00	1.0 1.00
PG 1512+370	5	$8.8^{+0.7}_{-0.0}$*	12.6	$8.8^{+0.3}_{-0.3}$*	10.9	8.95 ± 0.10[b]	14.2	12.6
		0.60 1.00		0.50 0.7			0.50 0.75	0.8 0.25
PG 1543+489	5	$9.5^{+0.0}_{-0.0}$	49.5	$8.3^{+0.5}_{-0.0}$	58.4	7.844[c]	573.1	420.9 (m)
		0.10 0.25		1.00 1.0			0.80 1.00	1.0 1.00
PG 1626+554	3	$8.8^{+0.0}_{-0.6}$*	12.5	$8.7^{+0.2}_{-0.4}$*	1.2 (m)	8.37[a]	15.4	4.3
		0.80 0.25		0.50 0.1			0.50 0.75	0.2 0.75

Fabian 2004) and broad iron lines are seen in several more AGN for which a relativistic disc line is a viable explanation (e.g. Mkn 766, Mason et al. 2003; Q0056-363, Porquet & Reeves 2003; Mkn 205, Reeves et al. 2001), our preliminary study of the broad-band SEDs of Laor PG quasars might suggest that a Schwarzschild geometry is more appropriate. In any case, the soft X-ray excess appears to be independent of the disc model.

6 DISCUSSION

The BQS is a well-studied sample and so there are various results in the literature with which to compare the *XMM–Newton* spectra. In particular, Laor et al. (1997) obtained values of the photon index for the 1.2–3.0 keV range that are comparable with the values we obtain for the softer of the two power laws, i.e. $\Gamma = 2.2$–3.7 below the break energy. We note that our derived break energies are in the range 0.9–2.6 keV, whereas in effect the Laor et al. study was equivalent to assuming a break energy >2 keV, and so this a reasonable but not exact comparison.[3] Comparison of the *XMM–Newton* and *ROSAT* photon indices is shown in the top panel of Fig. 6.

The BQS sample has also been observed previously at harder energies using the *ASCA* satellite. George et al. (2000) found a range $\Gamma = 1.5$–3.0, which is consistent with the *XMM–Newton* values for the Laor et al. sample. PG 1411+442 was the only source in the George et al. (2000) sample that could not be modelled successfully with a single power law in this range and, similarly, we have found that it warrants more detailed fitting than performed in this paper. *ASCA* data from a larger sample of 62 quasars was studied by Reeves & Turner (2000) and similar values obtained for Γ in the 2–10 keV range. Comparison of the *XMM–Newton* and *ASCA* photon indices is shown in the bottom panel of Fig. 6.

Table 8 provides a summary of X-ray properties of individual sources. In only four of the quasars studied in this paper (PG 1216+069, 1309+355, 1425+267 and 1440+356) could an additional neutral absorption component be detected. Warm absorbers have been discovered in the *XMM–Newton* spectra of PG 1114+445 and 1309+355 (Ashton et al. 2004) and possibly PG 1425+267 and 1411+442 (Ashton et al., in preparation). These findings are consistent with Laor et al. (1997), who identified a distinct group of 'X-ray-weak quasars' consisting of PG 1001+054, 1411+442 and 1425+267 on account of their absorption properties. We note that these same X-ray-weak objects are among the sources that show signs of UV absorption in their spectra (Laor & Brandt 2002). Reeves & Turner (2000) found absorption in just over half of their sources, mainly in the more distant objects but also in some of the low-redshift radio-loud quasars. In particular, they discuss possible warm absorber components in PG 1226+023 and 1425+267, again consistent with our results. This fraction of Laor sources with a warm absorber is notably less than the 50 per cent of a sample of Seyfert 1 galaxies (Reynolds 1997), as discussed by Laor et al. (1997) and Ashton et al. (2004).

We find little evidence for iron lines in the *XMM–Newton* spectra although the upper limits to the equivalent width allow for appreciable line emission in some other sources. Detections for which the equivalent width could be constrained (out to 99 per cent confidence) were obtained for just 12 sources but to low significance ($< 2\sigma$). Our upper limits are consistent with the *ASCA* results because Reeves & Turner (2000) report iron line detection in PG 1114+445, 1116+215, 1226+023 and 1425+267. We further note that Page et al. (2004a) detect weak iron emission in PG 1226+023 when they combine a series of nine observations together. Similarly our results are consistent with those of Porquet et al. (2004).

[3] For simplicity and comparison with the literature, we discuss the spectra in terms of their power-law parameters but note that the successful fitting of, for example, blackbody and Comptonization models to the soft X-rays by other authors may indicate a curved spectrum instead of a power law.

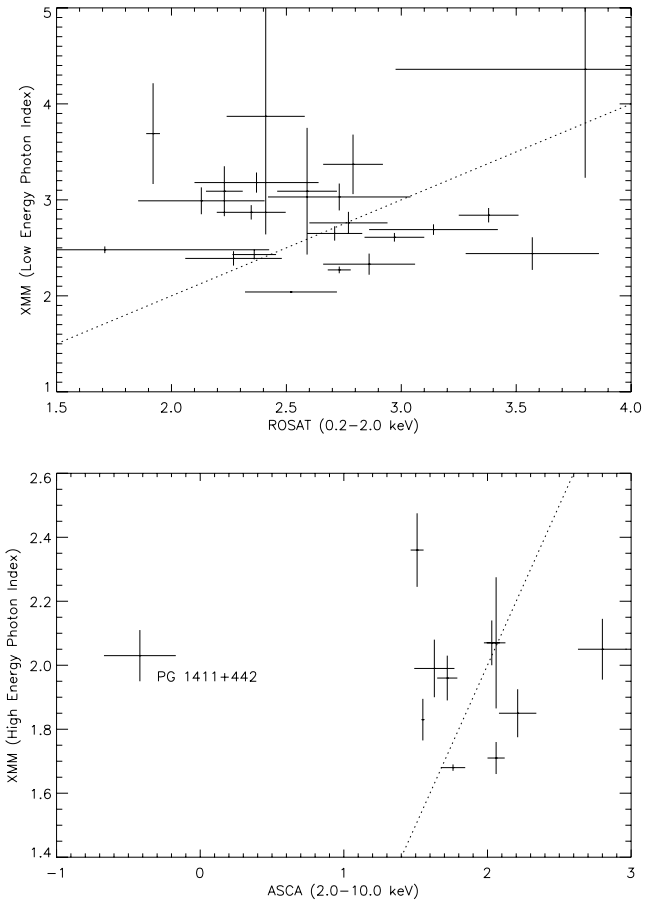

Figure 6. Comparison of the *XMM–Newton* photon indices with those of *ROSAT* (Laor et al. 1997; the energy indices quoted have been converted to photon indices) and *ASCA* (George et al. 2000; Reeves & Turner 2000). The dotted lines represent the point at which each pair of telescopes would obtain equivalent results.

On fitting a power law to the 2–5 keV range for each source, we find that there is a soft excess in each case where we do not find evidence for a warm absorber. This is in contrast to George et al. (2000) and Reeves & Turner (2000), who find a soft excess in just a few of their low-redshift quasars, although this is likely to be a reflection on the calibration of *ASCA* at low energies. Porquet et al. (2004) find more evidence for a soft excess component but, as also discussed by Page et al. (2004b), the derived blackbody temperatures are thought to be too hot to be direct emission from a thin accretion disc. Instead, they consider that UV disc photons are upscattered to X-ray energies via a Comptonizing medium. This is consistent with the correlations we find in Section 4: the strong correlation between the soft and hard power-law photon indices would suggest that the 0.3–10 keV emission is all produced by the same Comptonizing medium and not directly by the disc. In this case, the optical/X-ray continuum luminosity correlations would also be expected because an increase in accretion rate could lead to an increase in luminosity at all frequencies.

Table 8. Summary of the X-ray properties of each individual PG quasar.

PG 0947+396	Good fit to broken power law
PG 0953+414	Good fit to broken power law
PG 1001+054	Apparent good fit to broken power law (due to low count rate?) but discrepant parameters, 'X-ray weak quasar'
PG 1048+342	Good fit to broken power law
PG 1114+445	Poor fit to broken power law, warm absorber present
PG 1115+407	Good fit to broken power law, NLS1
PG 1116+215	Good fit to broken power law
PG 1202+281	Good fit to broken power law
PG 1216+069	Neutral absorption component required, although poor fit to broken power law
PG 1226+023	≡ 3C 273, radio-loud, highly luminous, neutral absorption component required, although poor fit to broken power law
PG 1309+355	Radio-loud, warm absorber present, good fit to broken power law
PG 1322+659	Good fit to broken power law
PG 1352+183	Good fit to broken power law
PG 1402+261	Reasonable fit to broken power law
PG 1411+442	Poor fit to broken power law, absorption and higher-energy component required, 'X-ray weak quasar'
PG 1415+451	Radio-loud, good fit to broken power law
PG 1425+267	Radio-loud, warm absorber probably present, good fit to broken power law but discrepant soft photon-index, 'X-ray weak quasar'
PG 1427+480	Good fit to broken power law
PG 1440+356	Reasonable fit to broken power law, neutral absorption required, NLS1
PG 1444+407	Good fit to broken power law
PG 1512+370	Good fit to broken power law
PG 1543+489	Broken power law provides good fit but poorly constrained, NLS1
PG 1626+554	Good fit to broken power law

It should therefore be possible to fit a Comptonized disc model to the optical–UV–X-ray region. In Section 5, we attempted to do this using the Czerny & Elvis (1987) model (both Kerr and Schwarzschild). While our fits would be much better constrained if we were able to sample the peak of the emission [presumably in the extreme-ultraviolet (EUV) range], some of the published mass estimates produce curves that are considerably less luminous than the observed optical/UV data.

However, aside from the mass estimates, it is clear that the accretion disc models presented here do not account for the soft X-ray excesses of these low-redshift quasars. This result, coupled with the correlation between the soft and hard X-ray slopes, leads us to question what sort of physical models *are* able to account for the observed spectra. If, as the tight correlation would suggest, the soft and hard X-ray parts of the spectra are produced via the same emission mechanism and in the same emitting region, it is likely that we are looking for a non-thermal mechanism, such as those invoking Comptonization and/or a synchrotron, as appears to be the case for the broad-band spectra of X-ray binaries in the low/hard state (e.g. Markoff, Falcke & Fender 2001). Models invoking thermal blackbody and/or bremsstrahlung components are non-physical at high energies and so the correlation would suggest that they are equally inappropriate at low energies. A two-temperature disc–corona model (such as Kawaguchi, Shimura & Mineshige 2001) requires the low- and high-energy power-law components to be produced in different regions and via different mechanisms, creating difficulty in producing such a tight correlation.

The failure of the accretion disc models to fit the soft X-ray spectrum also poses a possible problem for models of Narrow Line Seyfert 1 (NLS1) galaxies, which invoke an accretion disc with large inner radius for the soft X-ray excess (e.g. Pounds, Done & Osborne 1995). With Hβ line widths of 1000–2000 km s^{-1}, PG 1115+407, 1440+356 and 1543+489 can be classed as NLS1 objects: we find that these sources are more variable and have steeper spectra than most of the other sources in the sample, consistent with other NLS1 objects. However, the models yield considerably larger masses than the 10^6–10^7 M$_\odot$ that would be expected from NLS1 models. Alternative models for these objects might instead invoke a more face-on inclination angle and/or a more distant broad line region (e.g. Boller et al. 1992; Puchnarewicz et al. 1992; Wandel 1997).

We should question whether more complicated multiwavelength models are required. It is known that, like many quasars and active galaxies, PG 1226+023 (3C 273) has jets that emit at radio, optical and X-ray wavelengths (e.g. Courvoisier 1998 and references therein) and it is likely that the other radio-loud PG quasars have similar structures. Some radio-quiet quasars have now had their jets imaged at radio frequencies (e.g. Blundell, Beasley & Bicknell 2003) and, although none of the Laor radio-quiet objects has been resolved, they are emitting at significant flux densities of at least a few milli-Janskys. Fitting disc models to any source, for which a jet is making significant contributions to the optical or X-ray luminosity, will be meaningless.

Four of the sources studied here have a significant number of radio points from which we can determine the spectral index; of these, two are radio-loud (PG 1425+267 and 1512+370) and two are radio-quiet (PG 1116+215 and 1216+069).[4] Brocksopp et al. (2004) found that, for the radio-loud high-redshift quasar [HB89] 2000−330, the spectral index of the X-rays and radio emission were consistent and suggested that the X-ray emission might share a common origin with the radio, such as synchrotron self-Comptonization of jet photons. We see a similar relationship in just one of the low-redshift radio-loud objects studied in this paper, PG 1512+370. In contrast, for the two radio-quiet quasars studied here we find that the spectral indices of the X-rays are steeper than those of the radio. Conversely, the radio-loud quasar, PG 1425+267, has a steeper radio spectrum than X-ray. The radio spectral indices were in the range −0.6 to −0.9, consistent with optically thin emission. However, we also note that any curvature in the spectra may complicate comparison of the slopes and so a more thorough analysis should include study of the X-ray versus radio flux correlation. We will address this in a future work.

For these same four radio-loud sources, we also use the formulae of Marscher (1983) to estimate the amount of synchrotron self-Compton (SSC) emission expected at X-ray wavelengths, assuming that the radio emission was all emitted in a jet. We find that less than 1 per cent of the X-ray emission could be from such a source and so an even smaller fraction is to be expected in the radio-quiet sources. Therefore, we must look to alternative sources of X-ray emission and more sophisticated jet models in order to account for the observed spectra. For example, Zdziarski (1986) presents a model invoking

[4] However, we note that the concepts of 'radio-loud' and 'radio-quiet' may have been introduced artificially through obtaining quasar samples according to their optical properties and choosing specific radio observing frequencies (see e.g. Blundell 2003 and references therein).

SSC to explain the IR–X-ray spectra of radio-quiet AGN; similarly, the model of Falcke & Biermann (1995) produces a significant level of SSC at X-ray energies and may be applicable to radio-quiet objects as well as radio-loud. Again, we will be investigating these models in a future work.

7 CONCLUSIONS

We have analysed *XMM–Newton*/EPIC X-ray spectra for the Laor et al. sample of PG quasars and found that a model invoking a broken power law and iron line is an acceptable fit in the majority of cases. Those sources for which the model is a poor fit seem to require some sort of warm absorber at low energies and one source appears to need a further higher-energy component. These discrepant sources will be studied in more detail in a future paper. Iron lines were detected in a number of sources but with significance $< 2\sigma$. We have confirmed correlations between various optical and X-ray line/continuum parameters; in particular, we find that the power-law indices of the low- and high-energy power laws are well correlated, suggesting that both components have a common origin. We have also analysed *XMM–Newton*/OM photometry and combined this with the X-ray spectra and archive radio–UV photometry in order to compile broad-band SEDs. Fitting these spectra to a Comptonized disc model shows that the soft excess appears to be independent of the disc model, adding support to our interpretation of the correlation between the soft and hard X-ray spectra.

ACKNOWLEDGMENTS

We thank Ceri Ashton for useful discussion, Aneta Siemiginowska for the use of her accretion disc models and Gavin Ramsay for proof-reading the manuscript. This is work based on observations obtained with *XMM–Newton*, an ESA science mission with instruments and contributions directly funded by ESA Member States and the USA (NASA). We have made use of the NASA/IPAC Extragalactic Database (NED), which is operated by the Jet Propulsion Laboratory, California Institute of Technology, under contract with NASA.

REFERENCES

Arnaud K. A. et al., 1985, MNRAS, 217, 105
Arnaud K. A., 1996, in Jacoby G. H., Barnes J., eds, ASP Conf. Ser. Vol. 101, Astronomical Data Analysis Software and Systems V. Astron. Soc. Pac., San Francisco, p. 17
Ashton C. E., Page M. J., Blustin A. J., Puchnarewicz E. M., Branduardi-Raymont G., Mason K. O., Córdova F. A., Priedhorsky W. C., 2004, MNRAS, 355, 73
Baskin A., Laor A., 2005, MNRAS, 356, 1029
Blundell K. M., 2003, New Astron Rev., 47, 593
Blundell K. M., Beasley A. J., Bicknell G. V., 2003, ApJ, 591, L103
Boller T., Meurs E. J. A., Brinkmann W., Fink H., Zimmerman U., Adorf H.-M., 1992, A&A, 261, 57
Brandt W. N., Mathur S., Elvis M., 1997, MNRAS, 285, L25
Brocksopp C., Puchnarewicz E. M., Mason K. O., Córdova F. A., Priedhorsky W. C., 2004, MNRAS, 349, 687
Cardelli J. A., Clayton G. C., Mathis J. S., 1989, ApJ, 345, 245
Courvoisier T., 1998, A&AR, 9, 1
Czerny B., Elvis M., 1987, ApJ, 321, 305
Elvis M. et al., 1994, ApJS, 95, 1
Falcke H., Biermann P. L., 1995, A&A, 293, 665
George I. M., Turner T. J., Yaqoob T., Netzer H., Laor A., Mushotzky R. F., Nandra K., Takahashi T., 2000, ApJ, 531, 52
Gierliński M., Done C., 2004, MNRAS, 349, L7
Jester S. et al., 2005, AJ, 130, 873
Jiménez-Bailón E., Piconcelli E., Guainazzi M., Schartel N., Rodríguez-Pascual, Santos-Lleó M., 2005, A&A, 435, 449
Kawaguchi T., Shimura T., Mineshige S., 2001, ApJ, 546, 966
Kirsch M., 2003, EPIC status of calibration and data analysis. Online reference only (http://xmm.vilspa.esa.cs/docs/documents/CAL-TN-0018.pdf)
Kuraszkiewicz J. K. et al., 2003, ApJ, 590, 128
Laor A., 1990, MNRAS, 246, L369
Laor A., Brandt W. N., 2002, ApJ, 569, L641
Laor A., Fiore F., Elvis M., Wilkes B., McDowell J., 1994, ApJ, 435, 611
Laor A., Fiore F., Elvis M., Wilkes B., McDowell J. C., 1997, ApJ, 477, 93
Markoff S., Falcke H., Fender R. P., 2001, A&A, 372, L25
Marscher A. P., 1983, ApJ, 264, 296
Mason K. O. et al., 2001, A&A, 365, L36
Mason K. O. et al., 2003, A&A, 582, 95
Page K. L., Turner M. J. L., Done C., O'Brien P. T., Reeves J. N., Sembay S., Stuhlinger M., 2004a, MNRAS, 349, 57
Page K. L., Schartel N., Turner M. J. L., O'Brien P. T., 2004b, MNRAS, 352, 523
Peterson B. M., 1997, An Introduction to Active Galactic Nuclei. Cambridge Univ. Press, Cambridge
Piconcelli E., Jiménez-Bailón E., Guainazzi M., Schartel N., Rodríguez-Pascual P. M., Santos-Lleó M., 2005, A&A, 432, 15
Porquet D., Reeves J. N., 2003, A&A, 408, 119
Porquet D., Reeves J. N., O'Brien P., Brinkmann W., 2004, A&A, 422, 85
Pounds K. A., Done C., Osborne J. P., 1995, MNRAS, 277, L5
Puchnarewicz E. M., Mason K. O., Córdova F. A., Kartje J., Branduardi-Raymont G., Mittaz J. P. D., Murdin P. G., Allington-Smith J., 1992, MNRAS, 256, 589
Puchnarewicz E. M. et al., 1996, MNRAS, 281, 1243
Reeves J. N., Turner M. J. L., 2000, MNRAS, 316, 234
Reeves J. N., Turner M. J. L., Pounds K. A., O'Brien P. T., Boller Th., Ferrando P., Kendziorra E., Vercellone S., 2001, A&A, 365, L134
Reynolds C. S., 1997, MNRAS, 286, 513
Schmidt M., Green R. F., 1983, ApJ, 269, 352
Shields G. A., Gebhardt K., Salviander S., Wills B. J., Xie B., Brotherton M. S., Yuan J., Dietrich M., 2003, ApJ, 583, 124
Siemiginowska A., Kuhn O., Elvis M., Fiore F., McDowell J., Wilkes B. J., 1995, ApJ, 454, 77
Starling R. L. C., Siemiginowska A., Uttley P., Soria R., 2004, MNRAS, 347, 67
Sun W.-H., Malkan M. A., 1989, ApJ, 346, 68
Vaughan S., Fabian A. C., 2004, MNRAS, 348, 1415
Vestergaard M., 2002, ApJ, 571, 733
Wandel A., 1997, ApJ, 490, L131
Wilms J., Reynolds C. S., Begelman M. C., Reeves J., Molendi S., Staubert R., Kendziorra E., 2001, MNRAS, 328, L27
Zdziarski A., 1986, ApJ, 305, 45
Zheng W., Kriss G. A., Telfer R. C., Grimes J. P., Davidsen A. F., 1997, ApJ, 475, 469

This paper has been typeset from a TEX/LATEX file prepared by the author.